Laser-Based Metastable Krypton Generation

M. A. Dakka,[1] G. Tsiminis,[1,2] R. D. Glover,[3] C. Perrella,[1] J. Moffatt,[1,2] N. A. Spooner,[1,2,4]
R. T. Sang,[3] P. S. Light,[1] and A. N. Luiten[1,*]

[1]*Institute for Photonics and Advanced Sensing and School of Physical Sciences, University of Adelaide, SA 5000, Australia*
[2]*Cooperative Research Centre for Optimising Resource Extraction, School of Physical Sciences,
University of Adelaide, SA 5000, Australia*
[3]*Centre for Quantum Dynamics, School of Natural Sciences, Griffith University, QLD 4111, Australia*
[4]*Defence Science and Technology Group, PO Box 1500, SA 5111, Australia*

We demonstrate the generation of metastable krypton in the long-lived $1s^5$ state using laser excitation. The atoms are excited through a two-photon absorption process into the $2p^6$ state using a pulsed optical parametric oscillator laser operating near 215 nm, after which the atoms decay quickly into the metastable state with a branching ratio of 75%. The interaction dynamics are modeled using density matrix formalism and, by combining this with experimental observations, we are able to calculate photoionization and two-photon absorption cross sections. When compared to traditional approaches to metastable production, this approach shows great potential for high-density metastable krypton production with minimal heating of the sample. Here, we show metastable production efficiencies of up to 2% per pulse. The new experimental results gained here, when combined with the density matrix model we have developed, suggest that fractional efficiencies up to 30% are possible under optimal conditions.

Introduction.—Metastable noble gas atoms [1] have found wide use since the advent of laser manipulation of atoms, with diverse applications including atom lithography [2,3], rare isotope detection [4–6], Bose-Einstein condensation [7], optically pumped rare gas lasers [8], high resolution spectroscopy [9], and high precision fundamental physics experiments [10,11]. Metastable krypton (Kr*) itself finds use in krypton tagging velocimetry [12] and for radiokrypton dating [13–15].

These applications all require an experimental step to prepare the target into the relevant high energy (10–20 eV) metastable state. Primarily, direct-current (dc) and radio-frequency (rf) discharge sources are used [3,16–19], which are limited by poor (10^{-4}) average efficiency [20] and require a minimum gas density to operate. This minimum gas density requirement means that typically the discharge source is situated some distance from the experimental chamber and a series of specialized equipment is required to extract and transport the metastable atoms [21]. Previously all-optical approaches have been shown to circumvent this pressure requirement but have so far not demonstrated an increase in efficiency [22]. Furthermore, for applications where accurate measurements of the isotopic density of a sample is being measured, the sputtering of highly charged, electrostatically accelerated noble gas ions (11–25 eV) onto the surface of the vacuum chamber can lead to slow outgassing and unwanted cross contamination between samples [13]. Other production methods such as electron beam bombardment [23,24],

charge transfer [21,25], and optical pumping [22,26–29] are limited by space charge limitations, short source lifetimes due to sputtering, and reliance on initial discharge or electron-impact sources (inheriting some of the disadvantages of these sources), respectively [21].

The work here describes a direct optical excitation approach only possible using deep-UV (DUV) laser technology [30]. In this Letter we explore the parameter space for excitation conditions to optimize metastable production efficiency. This work is expected to avoid the major deficiencies of the discharge approaches—in particular, leading to higher efficiencies and also preventing sample cross contamination. Here we target a two-photon transition in krypton to access a high-lying excited state, which decays quickly (25 ns lifetime) into the desired metastable state with a high branching ratio ($\beta \approx 75\%$), although the level structures of all the noble gas species are equally suitable, provided a laser is available at the required wavelength. This Letter reports on a comprehensive investigation of pulsed Kr* production using a 215 nm laser by varying both the power and detuning of the laser excitation. We support observations with density matrix (DM) calculations that allow us to calculate the two-photon and photoionization cross sections.

Apparatus and procedure.—The approach of this work is shown on Fig. 1, where 215 nm light excites a two-photon transition into a short-lived $2p^6$ state. The 215 nm radiation is generated by frequency doubling, via second harmonic generation (SHG), a commercial optical parametric oscillator
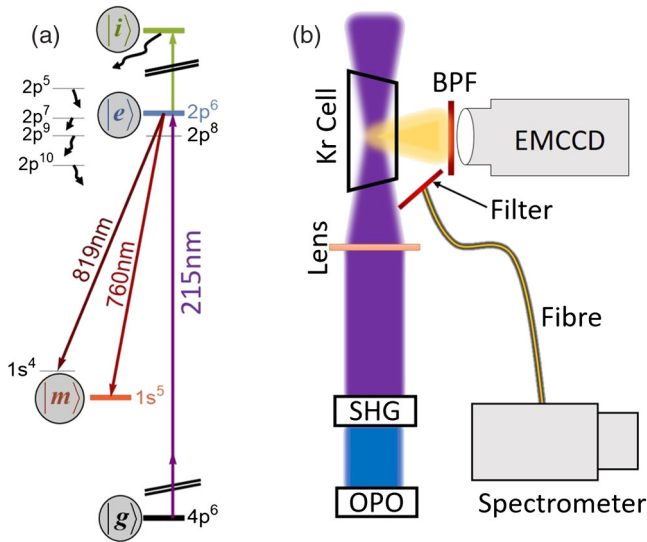
FIG. 1. (a) Partial energy level diagram of krypton. Levels in the theory section of this Letter are circled: ground $|g\rangle$, excited $|e\rangle$, metastable $|m\rangle$, ionized $|i\rangle$. (b) Laser-induced fluorescence detection apparatus.

FIG. 2. LIF spectra for pump energies E_p of 2 mJ (vertically offset by 0.2 for clarity) and 1 mJ, showing evidence of dissociative recombination peaks. The strongest measured recombination transitions are (a) $2p^9$-$1s^5$, (b) $2p^2$-$1s^2$, and (c) $2p^7$-$1s^4$. Branching ratio remains unchanged with varying laser energy.

(OPO) that can be tuned from 410–2500 nm. The output of the frequency-doubled OPO is a 5 ns DUV pulse with a maximum pulse energy E_p of 2 mJ over a 200 GHz bandwidth. The laser pulses are focused by a 75 mm CaF$_2$ lens to a 100 μm spot at the center of a quartz gas cell filled with krypton gas at a pressure of 0.05 mbar. The gas cell is sealed with uncoated 2° wedge windows made of UV grade SiO$_2$ that have been attached at an 11° angle to minimize back reflection. The UV pulse energy was directly monitored by intercepting the beam with a UV power meter, while the wavelength was ascertained by measuring the direct output of the OPO (at ∼429 nm) with a spectrometer.

Images of the laser-induced fluorescence (LIF) at 760 and 819 nm (from decay into the $1s^5$ and $1s^4$ states, respectively) are collected by an EMCCD camera positioned 95 mm from the laser beam focal region. To select between the two signals and reject scattered pump light and fluorescence from other decay routes, we have fitted 760 and 820 nm bandpass filters (BPF) with 10 nm FWHM to the front surface of an apochromatic camera lens. Assuming isotropic fluorescence, the total effective collection efficiency, including solid angle and losses in the optical collection system, is 0.1%. The signal-to-noise ratio of each image was improved by averaging 5 frames that were each of 5 s exposure time (a total of 250 pulses). In addition to the EMCCD measurements, a spectrometer with a suitable spectral filter collected the spectral content of the LIF via a multimode optical fiber.

In the circumstances prevailing in this experiment, the photoionization rate from the metastable state is negligible [31], and the low gas pressures (0.05 mbar) mean that the collisional rates are negligible in comparison to optical transition rates [16]. In those conditions, the 760 nm LIF is
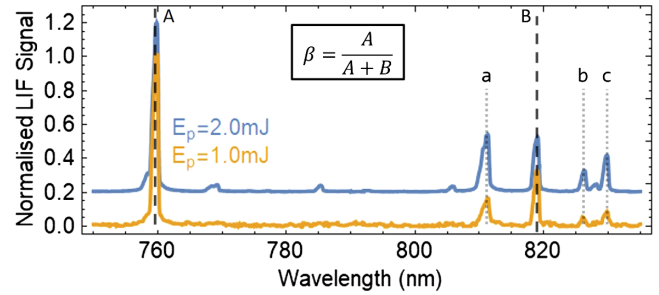
directly proportional to the total metastable population produced by a laser pulse. This gives us the means to produce a simple relation between the 760 nm LIF and the two-photon absorption cross section, $\sigma_0^{(2)}$.

Results.—We measured the spectral content of the LIF and noted multiple fluorescent peaks (Fig. 2). The branching ratio β out of the $2p^6$ excited state is calculated by taking the ratio of integrated intensities in the 760 and 819 nm LIF peaks, giving $\beta = (75 \pm 4)\%$. The uncertainty arises from uncertainty in the wavelength-dependent quantum efficiency of the spectrometer CCD. This value is consistent with literature values for this transition [26,27,32–40], but has an improved uncertainty (see Table I).

Additional peaks noted in the LIF spectrum arise from resonance-enhanced multiphoton ionization (REMPI) followed by dissociative recombination through the $5p$-$5s$ transition band [42]. As expected, these peaks disappear with lower excitation energy as shown in Fig. 2. The strongest such peaks come from decay channels via $2p^9$-$1s^5$ (811.5 nm), $2p^2$-$1s^2$ (826.5 nm), and $2p^7$-$1s^4$ (830.0 nm) transitions, labeled (a)–(c) in Fig. 2.

Figure 3 shows EMCCD images of the fluorescence intensity emitted from the side of the gas cell under a range of different input pulse energies. Although falling outside the central scope of this Letter, we observe a range of very interesting nonlinear behaviours at higher energies. The top image from panel (a) in Fig. 3 shows filamentation,

TABLE I. Comparing experiment to literature for Kr branching ratio and cross-section values.

Reference	β (%)	$\sigma_0^{(2)}$, (10^{-35} cm^4)	σ_{ei}, (10^{-18} cm^2)
This work	75 ± 4	5.2 ± 2.2	3.8 ± 1.0
Literature	76 ± 3 [a]	2.4 ± 0.8 (Xe)[b]	3.3 [c]

[a]Estimated uncertainty written here is the average deviation of the values, although quoted uncertainties are much larger [26,27,32–40].
[b]The ground-$2p^6$ transition of Xe. [41]. Not directly comparable.
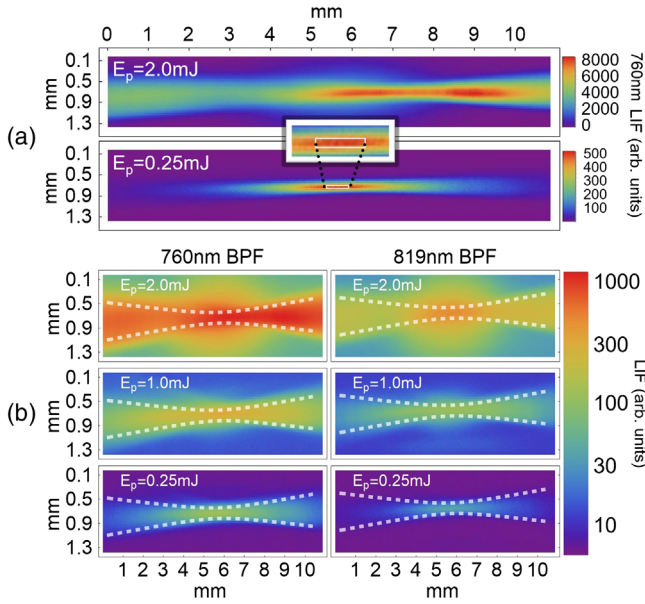[c]Calculated from Ref. [31].

FIG. 3. (a) LIF images at 760 nm (scaled linearly to highlight spatial features) showing evidence of filamentation at higher energies. Inset is an enlargement of the central region, with the analysis region in the white box. (b) Representative log scale images at 760 (left) and 819 nm (right) at 2.0, 1.0, and 0.25 mJ with e^{-2} beam diameter lines overlaid (white dotted). Beam propagation direction is left to right.

or refocusing, which occurs for laser intensities that rapidly (~ 1 ns) photoionize a significant fraction of the atoms within the laser beam [41]. We also note the halo shape surrounding the beam waist region [2 mJ images in Fig. 3(b) and more weakly in the 1 mJ images] that is likely due to space charge effects created by the intense pulse [43–45], and the subsequent (~ 5 μs) fluorescence from dissociative recombination [41].

In order to compare the experimental results to the theoretical model we translate the absolute photon counts from each EMCCD image into a total emitted photon number per pulse from a representative volume. This volume is centered on the waist and has boundaries set at the location that has an input intensity that is 90% of the maximum value [see Fig. 3(a)]. The emitted LIF photon number is then divided by the number of atoms (40×10^7 atoms) inside the interaction volume (6.0×10^{-6} cm^3) to yield an estimate of the LIF per atom ρ_{LIF} as a function of laser energy and detuning.

Theory and Analysis.—A time-dependent model of a 4-level system, using the state designations shown in Fig. 1(a), is used to calculate the metastable population $\rho_{mm}(t)$. The dynamics are described by the governing Liouville equation [46]:

$$\dot{\rho}_{ab}(t) = -\frac{i}{\hbar}[\hat{H}(t), \rho_{ab}(t)] + \hat{\mathcal{L}}(\gamma_k, \rho_{ab}(t)), \quad (1)$$

where $\hat{H}$ is the total interaction Hamiltonian and $\hat{\mathcal{L}}$ is the relaxation (Lindblad) operator where the γ_k term represents

relaxation rates. For $a = b$, $\rho_{aa} = |\langle a|a\rangle|^2$ is the probability of finding an atom in a given state $|a\rangle$, while for $a \neq b$, ρ_{ab} is the coherence term between states $|a\rangle$ and $|b\rangle$. In the scheme shown in Fig. 1(a), only the ρ_{eg} (and its conjugate) terms are nonvanishing, and since there are no intermediate states, the two-photon Rabi frequency $\Omega^{(2)}(t)$ can be related to the two-photon cross section $\sigma_0^{(2)}$ and the laser intensity $I(t)$ by [47,48]

$$\Omega^{(2)}(t) = \sqrt{\frac{2}{\pi}\sigma_0^{(2)}} \frac{I(t)}{\hbar\omega_0}, \quad (2)$$

where $\hbar$ is the reduced Planck constant and ω_0 is the laser frequency. The model takes account of laser detuning Δ, laser decoherence [49–51], collisional effects [16] including Penning ionization [52,53], spontaneous decay from the excited state [27], branching ratio, and photoionization. The photoionization rate from state $|a\rangle$ is related to the cross section σ_{ai} as

$$R_{ai} = \sigma_{ai} \frac{I(t)}{2\hbar\omega_0}, \quad (3)$$

where we note that the photoionization cross section from the $1s^5$ state σ_{mi} is less than 3% of that from the $2p^6$ state σ_{ei} [31]. We have thus neglected the former in the calculation as it does not significantly modify the metastable population.

For the relatively broad spectrum of the source used in this experiment, phase fluctuations (decoherence) play an important role in the excitation dynamics. We use the phase diffusion model [49–51] to average over these fluctuations, yielding a decoherence rate, γ_L,

$$\gamma_L = 2\sigma \frac{(b\sigma)^2}{(b\sigma)^2 + \Delta^2}, \quad (4)$$

where σ is the FWHM laser linewidth and b is a line shape parameter (0.5 for an ideal Lorentzian line shape and ~ 3 for the Gaussian line shape of the 200 GHz linewidth laser used in this experiment [50]).

Figure 4 shows a sample of the time evolution of population states under resonant excitation by a 5 ns, 0.25 mJ laser pulse with a beam diameter of 100 μm, and a gas pressure of 0.05 mbar.

Under these conditions, Kr* atoms are long-lived ($\gg 1$ μs) and thus we associate every detected 760 nm LIF photon with the production of a single Kr* atom. In this case, ρ_{LIF} is a direct measure of the steady-state fractional Kr* population $\rho_{mm}(t_{ss})$, where time $t = t_{ss}$ is long after pulse termination, and $\rho_{ee}(t_{ss}) \approx 0$. We note that the peak laser intensity used in this experiment (2 GW cm^{-2}) is well below the limit at which the laser field begins to exceed the binding energy of a valence Kr electron (a few PW cm^{-2}) and under the threshold for significant population redistribution to occur [54].
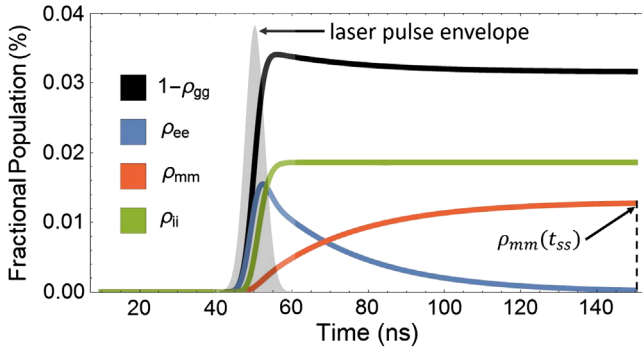
FIG. 4. Theoretical population dynamics for ground ρ_{gg}, excited ρ_{ee}, metastable ρ_{mm}, and ionized ρ_{ii} states at 0.05 mbar, excited by a 5 ns pulse centered at 50 ns (pulse envelope highlighted in gray) with $E_p = 0.25$ mJ.

We use the experimental data to derive the two-photon absorption cross section $\sigma_0^{(2)}$ and photoionization cross section from the $2p^6$ state σ_{ei} (see Table I) by a nonlinear fitting to the predictions of the density matrix model. The fitting approach is based on the minimum root mean squared error method by varying $\sigma_0^{(2)}$ and σ_{ei}. A comparison between experimental and theoretical results based on this approach is shown in Fig. 5, where we estimate to have achieved a maximum ρ_{LIF} of 2%.

We note the presence of some subtle line shape asymmetry as well as features on the low frequency wing in the experimental data of Fig. 5(c). These are repeatable and more pronounced when using medium and lower energy excitation. The origin of these effects is not definite although may be connected to subtle laser line shape changes in the excitation laser source when operated away from full power. These discrepancies represent small variations of the Kr* production rate at a large frequency detuning from resonance where the Kr* production rate is 2 orders of magnitude smaller than the on-resonance value. As such, they do not affect conclusions regarding the overall efficiency of a laser-based Kr* production scheme.

To the authors' knowledge, this is the only experimental measurement of the ground-$2p^6$ cross section in Kr, although we note that we obtain a similar value to that of the analogous transition in xenon [41] (see Table I). The derived photoionization cross section also agrees well with a previous theoretical estimate of this value [31].

Figure 6 shows extrapolation of theoretical Kr* production rates for three laser linewidths and varying pulse energies. In the low energy (< 200 μJ) and mid-to-large linewidth regime (10 and 200 GHz), the excitation rate is limited by the effective excitation energy and hence ρ_{mm} is proportional to E_p^2 as is expected from a two-photon process. For excitation using a laser with a Fourier transform limited linewidth (~ 250 MHz), 100 μJ is predicted to achieve 30% efficiency per pulse. In all cases, photoionization from the $2p^6$ state begins to dominate at high laser intensities, decreasing Kr* population. This shows that simply increasing the intensity does not necessarily lead to improved efficiency of Kr* production. The interplay between excitation, photoionization, and decay rates must be balanced to optimize Kr* production.

The maximum fractional metastable efficiency for the experimental conditions presented here is around 10^{-2} per pulse. In order to compare this efficiency to that of quasi-cw metastable generation sources (such as rf and dc discharge sources) one should properly consider the effective time averaged density of the metastable species. In the experiments reported above, this is relatively low because the collision-limited lifetime of the metastable atoms is a few microseconds at a pressure of 0.05 mbar, which is significantly below the interval between the excitation pulses
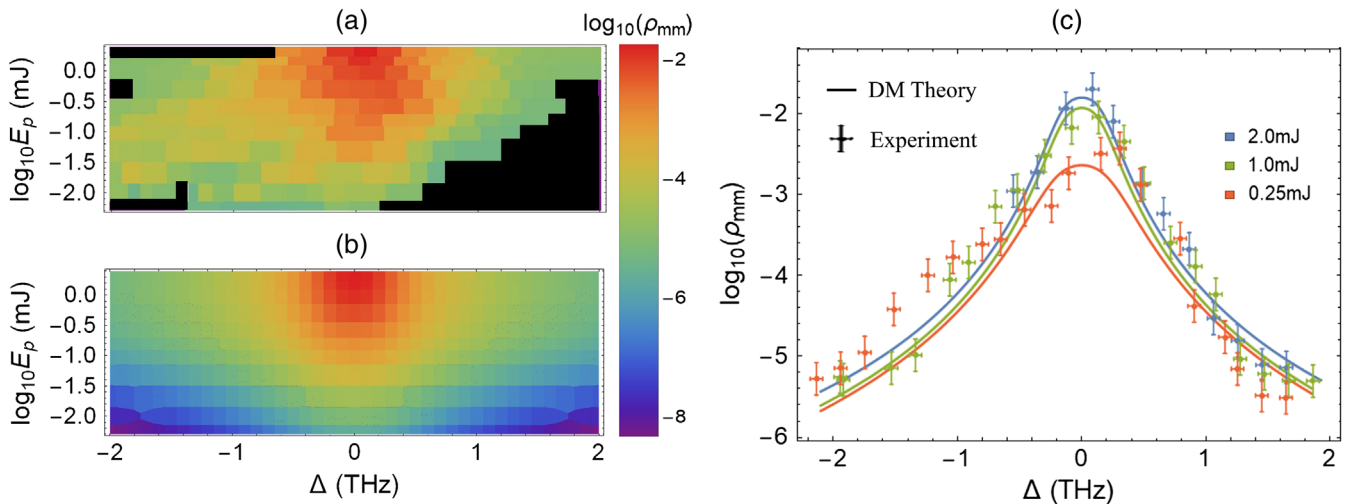

FIG. 5. (a) ρ_{LIF} (calculated from 760 nm LIF data) and (b) $\rho_{mm}(t_{ss})$ (fitted with theory) vs laser detuning, Δ, and energy, E_p. (c) Representative plots of experiment (points) vs theory (lines) at 2, 1.0, and 0.25 mJ.
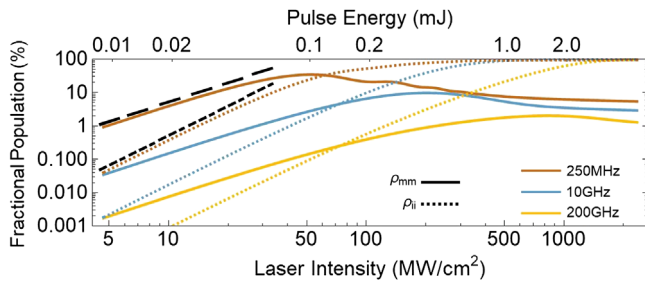
FIG. 6. Theoretical ρ_{mm} (solid) and ρ_{ii} (dashed) fractional populations vs laser intensity for several laser linewidths. In all cases the pulse duration is held at 5 ns. Intensity squared (long-dashed) and intensity cubed (short-dashed) lines are shown for reference.

(100 ms). Nonetheless, using the density matrix model we have developed here, combined with the new experimental values we have determined, allows us to predict a regime in which the metastable density of the laser approach can compete directly with the discharge approaches. Using laser parameters in the range of commercially available lasers (linewidth < 10 GHz, repetition rate ~ 10 kHz, and pulse energy ~ 10 μJ) together with a gas density below 1 μbar, predicts a fractional time-averaged density of Kr* above 10^{-4}, comparable with conventional sources.

Conclusion.—This Letter demonstrates that two-photon laser excitation is a viable method to achieve Kr* production efficiencies of $> 10^{-2}$ per pulse. We provide an experimental determination of the two-photon ground-$2p^6$ cross section, which is similar to that of a similar transition in xenon. The photoionization cross section, also determined experimentally, agrees well with previous literature.

These experiments show that by slightly modifying the excitation laser parameters and noble gas pressure, it will be possible to use laser approaches to produce a Kr* density comparable to that possible with discharge techniques; however, the resulting metastable atoms will have much lower average kinetic energy than those generated within a discharge plasma. This is critical for those applications in which one wants to produce the metastable atoms near to a laser cooling and trapping region, or where one wants to avoid driving ionized atoms into the surfaces of samples or the vacuum chamber.

*Corresponding author.
andre.luiten@adelaide.edu.au

[1] E. E. Muschlitz, Science **159**, 599 (1968).
[2] K. K. Berggren, A. Bard, J. Wilbur, J. Gillaspy, A. Helg, J. McClelland, S. Rolston, W. Phillips, M. Prentiss, and G. Whitesides, Science **269**, 1255 (1995).
[3] M. Baker, A. J. Palmer, W. R. MacGillivray, and R. T. Sang, Nanotechnology **15**, 1356 (2004).
[4] C. Y. Chen, Science **286**, 1139 (1999).
[5] W. Jiang, W. Williams, K. Bailey, A. M. Davis, S. M. Hu, Z. T. Lu, T. P. O'Connor, R. Purtschert, N. C. Sturchio, Y. R. Sun, and P. Mueller, Phys. Rev. Lett. **106**, 103001 (2011).
[6] Z.-T. Lu *et al.*, Earth-Sci. Rev. **138**, 196 (2014).
[7] A. Robert, O. Sirjean, A. Browaeys, J. Poupard, S. Nowak, D. Boiron, C. I. Westbrook, and A. Aspect, Science **292**, 461 (2001).
[8] W. T. Rawlins *et al.*, Opt. Exp. **23**, 4804 (2015).
[9] E. Altiere, E. R. Miller, T. Hayamizu, D. J. Jones, K. W. Madison, and T. Momose, Phys. Rev. A **97**, 012507 (2018).
[10] M. A. Player and P. G. H. Sandars, J. Phys. B. **3**, 1620 (1970).
[11] W. Vassen, C. Cohen-Tannoudji, M. Leduc, D. Boiron, C. I. Westbrook, A. Truscott, K. Baldwin, G. Birkl, P. Cancio, and M. Trippenbach, Rev. Mod. Phys. **84**, 175 (2012).
[12] N. J. Parziale, M. S. Smith, and E. C. Marineau, Appl. Opt. **54**, 5094 (2015).
[13] W. Jiang *et al.*, Geochim. Cosmochim. Acta **91**, 1 (2012).
[14] L.-Y. Tu, G.-M. Yang, C.-F. Cheng, G.-L. Liu, X.-Y. Zhang, and S.-M. Hu, Anal. Chem. **86**, 4002 (2014).
[15] Z.-T. Lu, Nat. Sci. Rev. **3**, 172 (2016).
[16] H. Katori and F. Shimizu, Phys. Rev. Lett. **70**, 3545 (1993).
[17] A. J. Palmer, M. Baker, and R. T. Sang, Rev. Sci. Instrum. **75**, 5056 (2004).
[18] A. J. Palmer, M. Baker, and R. T. Sang, Nanotechnology **17**, 1166 (2006).
[19] C.-F. Cheng, W. Jiang, G.-M. Yang, Y.-R. Sun, H. Pan, Y. Gao, A.-W. Liu, and S.-M. Hu, Rev. Sci. Instrum. **81**, 123106 (2010).
[20] X. Du, K. Bailey, Z.-T. Lu, P. Mueller, T. P. O'Connor, and L. Young, Rev. Sci. Instrum. **75**, 3224 (2004).
[21] F. B. Dunning and R. G. Hulet, *Atomic, Molecular and Optical Physics: Atoms and Molecules* (Academic Press, New York, 1996).
[22] M. Kohler, H. Daerr, P. Sahling, C. Sieveke, N. Jerschabek, M. B. Kalinowski, C. Becker, and K. Sengstock, Europhys. Lett. **108**, 13001 (2014).
[23] R. S. Freund, Rev. Sci. Instrum. **41**, 1213 (1970).
[24] M. A. Ali and P. M. Stone, Int. J. Mass Spectrosc. **271**, 51 (2008).
[25] R. H. Neynaber and S. Y. Tang, J. Chem. Phys. **70**, 4272 (1979).
[26] L. Young, D. Yang, and R. W. Dunford, J. Phys. B **35**, 2985 (2002).
[27] Y. Ding, S.-M. Hu, K. Bailey, A. M. Davis, R. W. Dunford, Z.-T. Lu, T. P. O'Connor, and L. Young, Rev. Sci. Instrum. **78**, 023103 (2007).
[28] H. Daerr, M. Kohler, P. Sahling, S. Tippenhauer, A. Arabi-Hashemi, C. Becker, K. Sengstock, and M. B. Kalinowski, Rev. Sci. Instrum. **82**, 073106 (2011).
[29] G. T. Hickman, J. D. Franson, and T. B. Pittman, Opt. Lett. **41**, 4372 (2016).

[30] C. A. Whitehead, B. D. Cannon, and J. F. Wacker, Appl. Opt. **34**, 3250 (1995).

[31] H. A. Hyman, Appl. Phys. Lett. **31**, 14 (1977).

[32] P.-T. Anne and J. E. Chamberlain, Proc. Phys. Soc. **82**, 133 (1963).

[33] P. W. Murphy, J. Opt. Soc. Am. **58**, 1200 (1968).

[34] D. A. Landman and R. Dobrin, Phys. Rev. A **8**, 1868 (1973).

[35] J. P. Lemoigne, X. Husson, and J. Margerie, Opt. Commun. **15**, 241 (1975).

[36] R. Lilly, J. Opt. Soc. Am. **66**, 245 (1976).

[37] W. E. Ernst et al., Physica (Amsterdam) **93C**, 136 (1978).

[38] M. Aymar and M. Coulombe, At. Data Nucl. Data Tables **21**, 537 (1978).

[39] R. S. F. Chang, H. Horiguchi, and D. W. Setser, J. Chem. Phys. **73**, 778 (1980).

[40] K. Dzierzega, U. Volz, G. Nave, and U. Griesmann, Phys. Rev. A **62**, 022505 (2000).

[41] S. Kroll and W. K. Bischel, Phys. Rev. A **41**, 1340 (1990).

[42] Y.-J. Shiu and M. A. Biondi, Phys. Rev. A **16**, 1817 (1977).

[43] E. W. McDaniel and E. A. Mason, The Mobility and Diffusion of Ions in Gases (John Wiley & Sons, New York, 1973).

[44] A. V. Tolmachev, B. H. Clowers, M. E. Belov, and R. D. Smith, Anal. Chem. **81**, 4778 (2009).

[45] P. N. B. Neves, C. A. N. Conde, and L. M. N. Tavora, J. Chem. Phys. **133**, 124316 (2010).

[46] K. Blum, Density Matrix Theory and its Applications (Springer, New York, 2012).

[47] D. Bates and B. Bederson, Advances in Atomic and Molecular Physics, Vol. 12 (Elsevier, New York, 1976).

[48] D. J. Bamford, A. P. Hickman, M. J. Dyer, and W. K. Bischel, J. Opt. Soc. Am. B **5**, 1369 (1988).

[49] G. S. Agarwal, Phys. Rev. Lett. **37**, 1383 (1976).

[50] P. Zoller and P. Lambropoulos, J. Phys. B **12**, L547 (1979).

[51] B.-N. Dai and P. Lambropoulos, Phys. Rev. A **34**, 3954 (1986).

[52] R. H. Neynaber and G. D. Magnuson, Phys. Rev. A **14**, 961 (1976).

[53] K. A. Temelkov, N. K. Vuchkov, and N. V. Sabotinov, J. Phys. Conf. Ser. **44**, 116 (2006).

[54] M. Shahidi, T. S. Luk, and C. K. Rhodes, J. Opt. Soc. Am. B **5**, 2386 (1988).